

Department of Electrical & Systems Engineering

Departmental Papers (ESE)

University of Pennsylvania

Year 2008

Dielectric sensing in ϵ -near-zero narrow waveguide channels

Andrea Alù*

Nader Engheta†

*University of Pennsylvania, andreaal@seas.upenn.edu

†University of Pennsylvania, engheta@seas.upenn.edu

Copyright 2008 American Institute of Physics. This article may be downloaded for personal use only. Any other use requires prior permission of the author and the American Institute of Physics. Reprinted in *Physical Review B*, Volume 78, Article 045102, July 2008. Publisher URL: <http://dx.doi.org/10.1103/PhysRevB.78.045102>

This paper is posted at ScholarlyCommons.

http://repository.upenn.edu/ese_papers/427

Dielectric sensing in ϵ -near-zero narrow waveguide channels

Andrea Alù and Nader Engheta*

Department of Electrical and Systems Engineering, University of Pennsylvania, Philadelphia, Pennsylvania 19104, USA

(Received 28 May 2008; published 3 July 2008)

We exploit here the dramatic field enhancement caused by energy squeezing and tunneling (i.e., “supercoupling”) in metamaterial-inspired ultranarrow waveguide channels with near-zero effective permittivity in order to sense small permittivity variations in a tiny object. The supercoupling effect is accurately modeled analytically and closed-form expressions are derived to describe the presence of defects or permittivity perturbations along the channel. Applications for tailoring its pass-band frequency and for high- Q sensing are proposed at microwave frequencies.

DOI: [10.1103/PhysRevB.78.045102](https://doi.org/10.1103/PhysRevB.78.045102)

PACS number(s): 41.20.Jb, 42.82.Et, 52.40.Db, 52.40.Fd

I. INTRODUCTION

The possibility of squeezing energy through subwavelength apertures and channels has been recently investigated in several systems and setups involving plasmonic materials and metamaterials (see, e.g., Refs. 1–3). Somewhat analogous to these findings, the idea of metamaterial supercoupling, i.e., energy squeezing and tunneling through subwavelength narrow waveguide channels of arbitrary length and narrow height filled with ϵ -near-zero (ENZ) metamaterials, has been put forward in a recent letter.⁴ Further theoretical results and experimental realization of this anomalous phenomenon have been obtained,^{5–7} demonstrating how it is possible to induce such tunneling in various waveguide configurations at microwave frequencies. In particular, we have reported in Refs. 5 and 6 how the same tunneling phenomenon may be achieved inside a simple hollow rectangular channel of narrow height that operates near the cutoff frequency of its dominant TE_{10} mode, thus making use of its natural dispersion to mimic the response of ENZ materials.^{8,9} This may lead to resonant transmission and vanishingly small phase delay through arbitrarily narrow waveguide channels, independent of their total length and geometry.

As reported and discussed in Refs. 4–7, this energy squeezing is associated with a huge increase in the magnitude of the electric field inside the ENZ channels. Intuitively, one can expect that such high-intensity field may ensure high sensitivity to small variations in material parameters, which may then be exploited for material sensing applications. Here we analyze in detail the perturbative effects of a small defect (e.g., a small change in material permittivity) or of a small cavity carved inside the metamaterial channel, with particular attention to the resulting changes in the channel tunneling properties. In particular, in the case of high-quality-factor (i.e., high- Q) tunneling, it is shown how the high-intensity electric field in the channel may be successfully used for accurate sensing applications and for fine tuning of the tunneling mechanism.

II. THEORETICAL ANALYSIS AND NUMERICAL RESULTS

Consider the geometry of Fig. 1, consisting of an ultranarrow rectangular channel, of height a_{ch} and length L , con-

necting the two sections of a waveguide of height $a \gg a_{ch}$. All the waveguide sections have the same width $b > a$, which tailors the dispersion properties of the fundamental TE_{10} mode. In particular, the TE_{10} propagation constant in each section of the waveguide may be regarded as that of a TEM wave propagating in an unbounded medium or in a parallel-plate waveguide with effective constitutive parameters,⁸

$$\begin{aligned} \epsilon_{\text{eff}}/\epsilon_0 &= \epsilon - c^2/(4f^2b^2), \\ \mu_{\text{eff}} &= \mu_0, \end{aligned} \quad (1)$$

where ϵ is the permittivity of the homogeneous material filling the waveguide section, c is the velocity of light in free space, and an $e^{-i2\pi ft}$ time convention has been assumed. At the cutoff frequency of this mode, i.e., when $b = \lambda/2$ with λ being the wavelength in the filling material with permittivity ϵ , the effective permittivity (1) “experienced” by the mode is zero, consistent with the infinite phase velocity of a cutoff mode or of a TEM wave in an ENZ metamaterial. This direct analogy may be exploited to realize metamaterial effects in several geometries (see, e.g., Refs. 8 and 9). Metamaterials realized with this technique are inherently robust to losses, since they avoid the use of small inclusions typical of con-

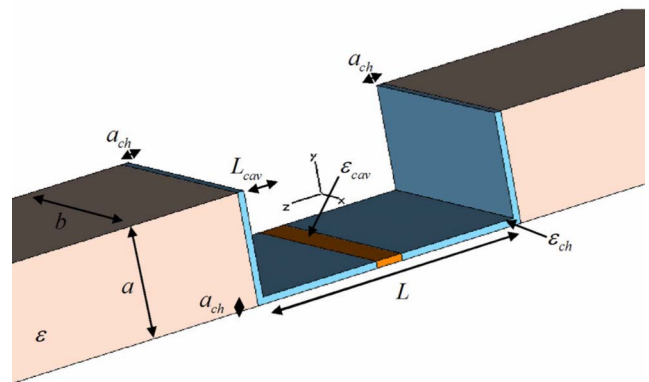


FIG. 1. (Color online) Geometry of the structure proposed as a permittivity sensor. The two input and output rectangular waveguides are connected via an ultranarrow channel (shown in blue). In the middle, an object (i.e., a cavity region) with permittivity ϵ_{cav} different from that of the channel is inserted. The structure is all surrounded by conducting walls.

ventional metamaterial technology, which usually lead to absorption and radiation losses associated with technological imperfections and disorder.

As we have done in Ref. 6, this technique may be applied to experimentally verify the anomalous properties of effective ENZ channels for resonant tunneling and zero-phase enhanced transmission, in principle independent of their geometry and length. In the geometry of Fig. 1 we have also considered two narrow sections of length a_{ch} attached to the channel, with the aim of “matching” the incident mode into the narrow channel, forming a characteristic U shape for the ENZ region (blue region in Fig. 1).

In this way, we may obtain the ENZ-related supercoupling effects^{4–6} using conventional materials, e.g., a dielectric or even free space with $\epsilon_{ch} = \epsilon_0$, filling the U channel. Since the ENZ-based tunneling is expected to occur at the cutoff frequency of the narrow channel, it is sufficient to have the remaining part of the waveguide filled with a regular dielectric with $\epsilon > \epsilon_{ch}$ to ensure propagation in these outer sections of the waveguide at this frequency. The phase delay between the entrance and the exit of the narrow channel is expected to remain very small, independent of the channel length, due to the infinite phase velocity of the mode near its cutoff, resulting in a uniform and strongly enhanced electric field along the channel.

Now we consider a small cavity region with length L_{cav} and permittivity $\epsilon_{cav} \neq \epsilon_{ch}$ in the channel (Fig. 1). The presence of this cavity region with a permittivity different from the rest of the channel clearly perturbs the tunneling effect. In Ref. 6, we have studied the effects of an air cavity in the ENZ narrow channel on the electric- and magnetic-field distributions in the channel. Here we concentrate on how and to what extent the cavity with $\epsilon_{cav} \neq \epsilon_{ch}$ may alter and tune the tunneling and supercoupling aspects of the ENZ channel. As it will be shown in the following, this analysis may provide us with quantitative measures of the perturbation caused by the presence of a small object (here a cavity) of permittivity ϵ_{cav} . This may directly lead us to useful applications of this setup for sensing dielectric properties of an object under test.

The overall system of Fig. 1 may be analyzed using a transmission-line (TL) model, consistent with the one presented in Ref. 7 for a different geometry of the supercoupler, since each waveguide section supports the same dominant TE₁₀ mode.¹⁰ In particular, each section is described by its characteristic impedance $\eta = \sqrt{\mu_0/\epsilon_{eff}}$ and wave number $\beta = 2\pi f\sqrt{\mu_0\epsilon_{eff}}$, and the steps in the U channel cross section may be modeled with voltage transformers with a transform ratio $s = a_{ch}/a$ and parallel reactive loads that take into account the localized higher-order evanescent mode excitation. In this specific geometry, since the steps are embedded in an effective ENZ region (the U channel) at the resonant frequency, these parallel loads may be neglected, since the con-

dition $\epsilon_{eff} \approx 0$ implies an extremely high impedance for these loads.¹¹ Similarly, due to the condition $a_{ch} \ll 2\pi/\beta_{ch}$, it is possible to neglect the presence of the small lateral transition regions of the U in the TL model. We note that this same model (and the following discussions) applies for a parallel-plate waveguide when filled with metamaterials with permittivity ϵ_{eff} , consistent with the geometry in Ref. 4.

In the absence of the cavity, or when $\epsilon_{cav} = \epsilon_{ch}$, the input impedance at the entrance of the channel may be written as

$$Z_{in} = \frac{2s^2\eta_{ch}^2\eta_{out} - is\eta_{ch}(s\eta_{ch} - \eta_{out})(s\eta_{ch} + \eta_{out})\sin(2\beta_{ch}L)}{s^2\eta_{ch}^2 + \eta_{out}^2 + (s\eta_{ch} - \eta_{out})(s\eta_{ch} + \eta_{out})\cos(2\beta_{ch}L)}, \quad (2)$$

where the subscripts *ch* and *out* refer to the channel and the outside region, respectively. Total transmission is obtained when $Z_{in} = \eta_{out}$, i.e., either when $L = 2\pi/\beta_{ch}$ or when

$$\eta_{ch} = \pm \frac{\eta_{out}}{s}. \quad (3)$$

The first solution corresponds to classic Fabry-Perot resonances of the channel, very sensitive to the length of the channel and the frequency of operation, whereas condition (3) is a unique matching condition obtainable only near the channel cutoff frequency, which is interestingly independent of its geometry (and in particular its length). The strong mismatch at the entrance and exit faces of the channel, due to the difference in heights, is compensated by the huge increase in its characteristic impedance for frequencies right above the cutoff. In the limit of $a_{ch} \rightarrow 0$, i.e., $s \rightarrow 0$, condition (3) requires the system to operate at the frequency for which $\epsilon_{eff} = 0$, i.e., at the channel’s cutoff frequency, independent of the channel length. This is consistent with the theoretical results obtained in this limiting case in Ref. 4 using a different approach. For finite but narrow enough channels ($s \approx 0$), Eq. (3) suggests operation at frequencies for which $\epsilon_{eff} \approx 0^+$. It should be mentioned that the steep variation of η_{ch} right above the cutoff frequency implies that the tunneling frequency indeed occurs very close to the cutoff frequency, irrespective of variations in a_{ch} (while $a_{ch} \ll a$), consistent with the theoretical and experimental results in Refs. 4–7. The presence of the parallel loads, representing the *E*-plane discontinuities, would slightly shift down the tunneling frequency,¹¹ but they do not notably affect the main features in this scenario. The low value of ϵ_{eff} in the channel implies $\beta_{ch} \approx 0$, which ensures small phase delay and uniform field inside the channel, whereas the continuity of voltage across the step leads to an enhancement of the electric field inside the channel by a factor of $1/s$ with respect to the field in the outer waveguide sections.

Consider now a small cavity region with permittivity $\epsilon_{cav} \neq \epsilon_{ch}$ in the narrow channel, as depicted in Fig. 1. Applying the same TL model, condition (3) is modified into

$$\eta_{ch}^2 \left(1 + \frac{2 \sin[\beta_{cav}L_{cav}](\eta_{cav}^2 - \eta_{ch}^2)}{\{(\eta_{ch}^2 - \eta_{cav}^2 + (\eta_{ch}^2 + \eta_{cav}^2)\cos[\beta_{ch}(L - L_{cav})])\sin[\beta_{cav}L_{cav}] + 2\eta_{cav}\eta_{ch} \cos[\beta_{cav}L_{cav}]\sin[\beta_{ch}(L - L_{cav})]\}} \right) = \frac{\eta_{out}^2}{s^2}, \quad (4)$$

where the subscript *cav* refers to the cavity parameters. For the sake of simplicity, but without loss of generality, we have assumed that the cavity is positioned in the center of the channel. Equation (4) quantifies the perturbation and the shift in the tunneling frequency caused by the cavity. In particular, it may be deduced from Eq. (4) that the shift is always toward lower frequencies if $\epsilon_{cav} > \epsilon_{ch}$, implying that when the cavity is inserted the tunneling occurs at a frequency lower than the channel's cutoff frequency. It is interesting to point out that for this symmetric scenario, for which the cavity is placed at the center of the channel, total transmission can still be achieved when Eq. (4) is satisfied. For the asymmetric case, however, the resonant tunneling does not ensure, in general, total transmission.

Figure 2 shows the transmission coefficient predicted using the analytical TL model described above (dashed line) and compared with the full-wave numerical simulations¹² (solid lines) for different geometries of the channel and the cavity. In all these examples $L=127$ mm, $b=2a=101.6$ mm, $\epsilon=2\epsilon_0$ (the permittivity of Teflon), and $\epsilon_{ch}=\epsilon_0$. The black lines refer to the case in which the cavity has the same permittivity as the channel, i.e., $\epsilon_{cav}=\epsilon_{ch}=\epsilon_0$, which is consistent with the geometry analyzed in Ref. 6. The ENZ-related tunneling occurs very close to the cutoff frequency of the channel, which happens at $f=1.48$ GHz in this scenario. A second peak, consistent with a Fabry-Perot resonance, is obtained at a higher frequency, but this is strongly dependent on the length L .

Figure 2(a) considers the presence of a cavity with $L_{cav}=L/10$ in a channel with $a_{ch}=a/64$. Small variations in ϵ_{cav} introduce a significant shift in the ENZ-related tunneling frequency, in accordance with Eq. (4). The full-wave numerical simulations agree very well with the analytical model derived above (which neglects the presence of reactive loads describing the steps around this tunneling frequency), validating the assumption that the presence of an effective ENZ region around the channel E -plane discontinuities significantly reduces the excitation of higher-order evanescent modes.¹¹ At a higher frequency, however, when the Fabry-Perot resonance arises (for this geometry around 1.8 GHz) and the channel has a larger positive ϵ_{eff} , the presence of these loads cannot be safely neglected, as revealed in the disagreement between the analytical and simulation lines around this frequency. We note here that the high- Q ENZ-related transmission peak in the channel may be fine tuned by varying the cavity permittivity ϵ_{cav} around the tunneling frequency. However, the Fabry-Perot resonance peak, in comparison, is weakly affected by the presence of the cavity due to the nonuniform distribution of electric field in the channel in the Fabry-Perot scenario. In particular, in this case the electric-field distribution is such that the field is expected to be near zero in the center of the channel where the cavity is positioned.

Figure 2(b) considers a similar geometry but with a channel with higher height, i.e., $a_{ch}=a/16$. In this case the electric-field enhancement in the channel is less, and correspondingly the Q of the tunneling transmission is also lowered, causing broadening of bandwidth of transmission peaks. Figure 2(c) presents the results for a larger cavity, i.e.,

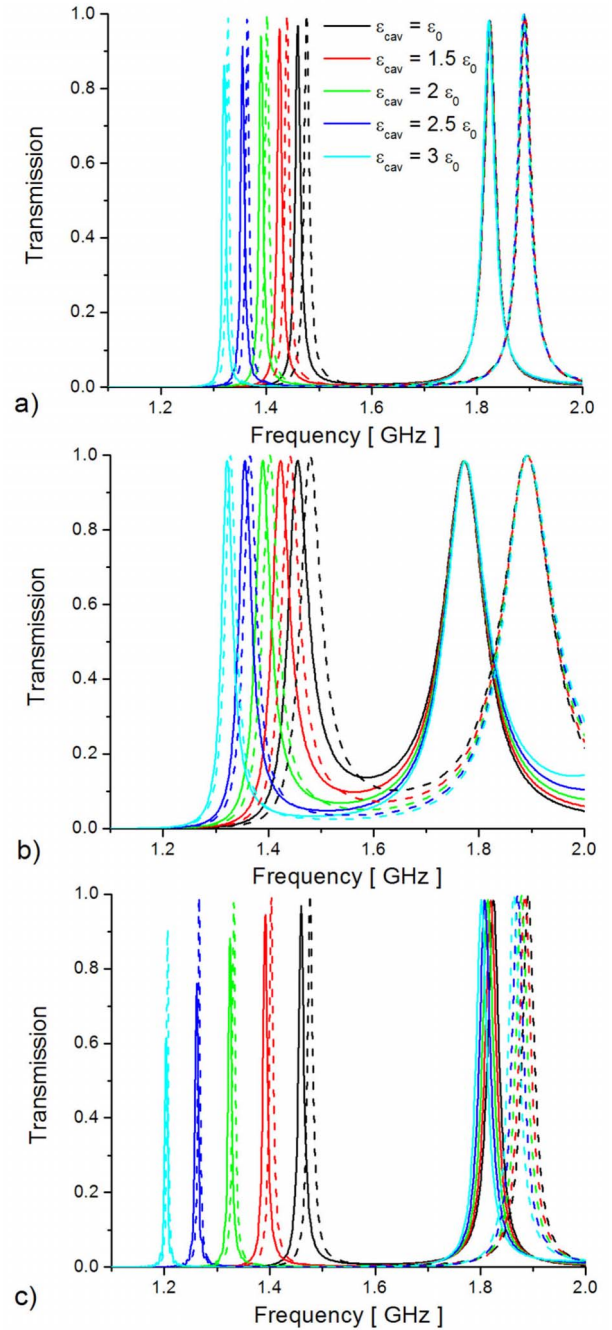


FIG. 2. (Color online) Transmission coefficient for the U channel of Fig. 1 with $L=127$ mm, $b=2a=101.6$ mm, $\epsilon=2\epsilon_0$, and $\epsilon_{ch}=\epsilon_0$: (a) $a_{ch}=a/64$, $L_{cav}=L/10$; (b) $a_{ch}=a/16$, $L_{cav}=L/10$; and (c) $a_{ch}=a/64$, $L_{cav}=L/5$. Solid lines: full-wave simulations (Ref. 12); dashed lines: TL model.

$L_{ch}=L/5$. In this case the resonance shift is more pronounced, as expected from the larger geometrical perturbation, but maintaining a similar Q factor as in the case of Fig. 2(a), since a_{ch} remains unchanged.

These results are summarized in Fig. 3, which reports the calculated shift of tunneling frequency [Fig. 3(a)] and the variation of the transmission coefficient at the channel cutoff frequency [Fig. 3(b)] for the three geometries of Fig. 2. This

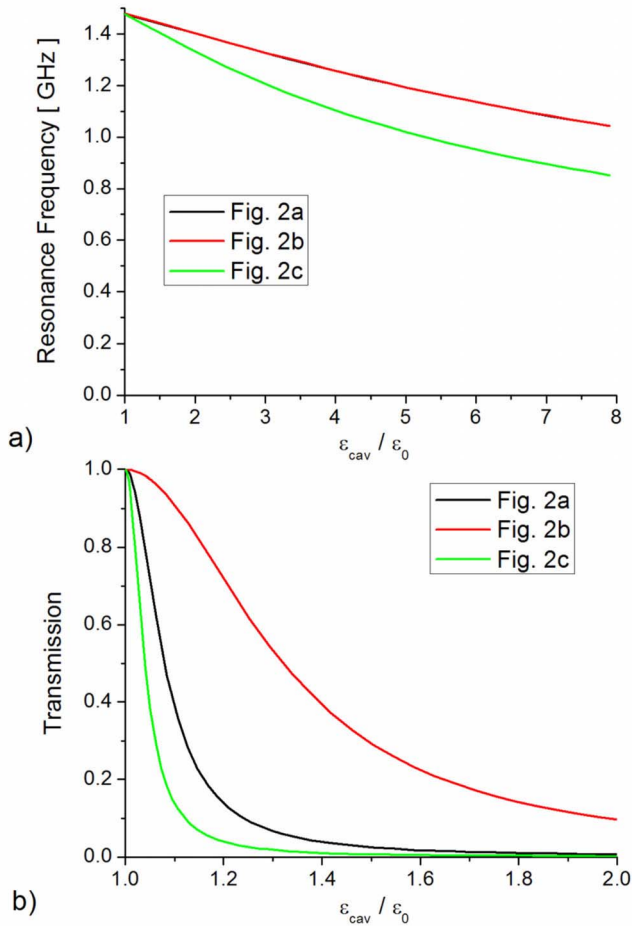


FIG. 3. (Color online) Variation of (a) the ENZ-related tunneling frequency and (b) the ENZ-related transmission coefficient at the channel's cutoff frequency $f=1.48$ GHz vs normalized ϵ_{cav} for the geometries of Fig. 2.

clearly reveals the filtering response of this ENZ-related tunneling phenomenon and suggests that the ENZ-inspired supercoupling may be exploited as a sensor for permittivity measurement by properly tailoring the tunneling Q factor. Operating at the channel's cutoff frequency, the transmission coefficient can be sensitively altered when a small object (particle, fluids, etc.) with permittivity ϵ_{cav} is inserted in the channel. By measuring this transmission coefficient, one can then evaluate the value of ϵ_{cav} , based on a curve such as Fig. 3(b). We have assumed here that ϵ_{cav} is a real quantity, since losses in dielectric materials may be safely neglected in this context, but this analysis remains valid also for absorbing materials.

Figure 4 shows the electric- and magnetic-field distributions, normalized to the impinging field amplitude, calculated on the bottom plate of the waveguide across the channel for the geometries in Figs. 2(a) and 2(c) with $\epsilon_{cav}=3\epsilon_0$ at the corresponding resonant frequencies, as indicated in the caption. It is clear that we have a large increase in the normalized electric-field distribution inside the cavity, even more than what is attainable within an empty supercoupling channel at its cutoff frequency, which for these geometries would correspond to a uniform distribution all across the

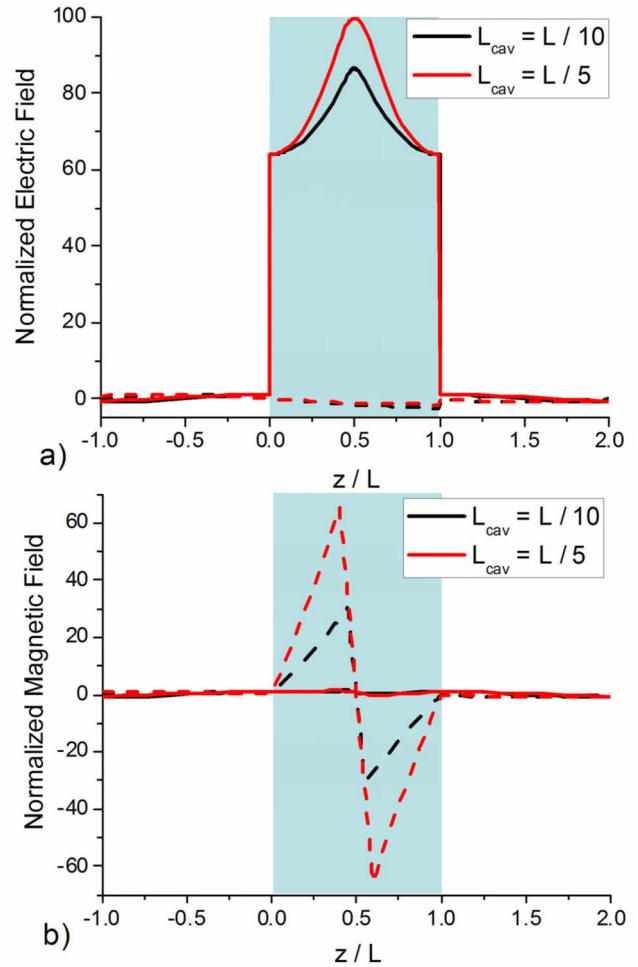


FIG. 4. (Color online) Normalized (a) electric-field E_y and (b) magnetic-field H_x distributions [real (solid) and imaginary (dashed) part] on the bottom plate of the waveguide at the tunneling frequencies $f=1.327$ GHz and $f=1.206$ GHz, respectively, for the geometries of Figs. 2(a) and 2(c) with $\epsilon_{cav}=3\epsilon_0$. The channel region is highlighted in the plots.

channel with normalized amplitude equal to $s=64$. With the cavity included, however, the electric field is further increased in the central region of the channel, where the cavity is placed, due to an anomalous growing exponential tail in the first part of the channel associated with resonant tunneling and the fact that the channel is resonating below its cutoff. This is even more evident in the magnetic-field distribution [Fig. 4(b)], which would be constant in an empty ENZ channel.⁴ The downshift of the tunneling frequency produces a large buildup of the normalized electromagnetic fields in the channel, localized at the cavity edges. In some sense, this is analogous to the exponential growth of the electromagnetic fields in the resonant pairs of metamaterials below cutoff,¹³ even if in this scenario the resonance interestingly happens in a simple hollow waveguide section. The field increase is more pronounced for a larger cavity, since the resonance happens at lower frequencies for which the effective permittivity of the channel is more negative, following Eq. (1).

III. CONCLUSIONS

We have reported here an idea to exploit the dramatic field enhancement associated by energy squeezing and tunneling in metamaterial-inspired ultranarrow waveguide channels with near-zero effective permittivity in order to sense small permittivity variations in a tiny object. We have analytically modeled the supercoupling effect, deriving closed-form expressions to describe the perturbation caused by presence of defects or permittivity perturbations along the channel. The experimental microwave realization of dielec-

tric sensing presented in this paper is currently under test in our group, and the extension of these concepts to optical frequencies is also conceptually viable using plasmonic waveguide channels. Applications for tuning the supercoupling pass-band frequency and for high- Q sensing are envisioned in different frequency regimes

ACKNOWLEDGMENT

This work was supported in part by the U.S. Office of Naval Research (ONR) under Grant No. N 00014-07-1-0622.

*Author to whom correspondence should addressed; engheta@ee.upenn.edu

¹T. W. Ebbesen, H. J. Lezec, H. F. Ghaemi, T. Thio, and P. A. Wolff, *Nature* (London) **391**, 667 (1998).

²D. E. Grupp, H. J. Lezec, T. Thio, and T. W. Ebbesen, *Adv. Mater.* (Weinheim, Ger.) **11**, 860 (1999).

³A. Alù, F. Bilotti, N. Engheta, and L. Vegni, *IEEE Trans. Antennas Propag.* **54**, 1632 (2006).

⁴M. G. Silveirinha and N. Engheta, *Phys. Rev. Lett.* **97**, 157403 (2006).

⁵M. G. Silveirinha and N. Engheta, *Phys. Rev. B* **75**, 075119 (2007).

⁶B. Edwards, A. Alù, M. E. Young, M. Silveirinha, and N. Eng-

heta, *Phys. Rev. Lett.* **100**, 033903 (2008).

⁷R. Liu, Q. Cheng, T. Hand, J. J. Mock, T. J. Cui, S. A. Cummer, and D. R. Smith, *Phys. Rev. Lett.* **100**, 023903 (2008).

⁸W. Rotman, *IRE Trans. Antennas Propag.* **10**, 82 (1962).

⁹R. Marques, J. Martel, F. Mesa, and F. Medina, *Phys. Rev. Lett.* **89**, 183901 (2002).

¹⁰T. Rozzi and M. Mongiardo, *IEEE Trans. Microwave Theory Tech.* **39**, 1279 (1991).

¹¹A. Alù, M. G. Silveirinha, and N. Engheta, *Phys. Rev. E* (to be published).

¹²CST Microwave Studio, 2006B (www.cst.com).

¹³A. Alù and N. Engheta, *IEEE Trans. Antennas Propag.* **51**, 2558 (2003).